Available online at www.sciencedirect.com
ScienceDirect
Applied Catalysis B: Environmental 78 (2008) 342–354
APPLIED CATALYSIS B: ENVIRONMENTAL
www.elsevier.com/locate/apcatb

N_2O decomposition over wet- and solid-exchanged Fe-ZSM-5 catalysts

Joo-Hyoung Park [a], Jong-Hyun Choung [a], In-Sik Nam [a,*], Sung-Won Ham [b]

[a] *School of Envi. Sci. & Eng./Department of Chem. Eng., Pohang University of Science and Technology, Pohang, Republic of Korea*
[b] *Department of Chem. Eng., Kyungil University, Kyungsan, Republic of Korea*

Received 2 April 2007; received in revised form 17 September 2007; accepted 18 September 2007
Available online 21 September 2007

Abstract

The N_2O decomposition activity of Fe-ZSM-5 strongly depends on the iron content and the preparation methods, including wet (WIE) and solid state ion exchanges (SSIE). The state of Fe species formed on the surface of a series of Fe-ZSM-5 catalysts containing a variety of Fe contents with respect to the preparation method and their role for N_2O decomposition activity have been systematically examined. The general trend for the decomposition activity of Fe-ZSM-5-SSIE is higher than that of Fe-ZSM-5-WIE, indicating the formation of a distinctive local structure of Fe on the catalyst surface during the course of the ion-exchange procedure. Based upon the Fourier transformed Fe K-edge EXAFS spectra for the series of Fe-ZSM-5-SSIE and -WIE catalysts, most of the Fe species on the surface of Fe-ZSM-5-SSIE with high Fe loading are well dispersed in the form of oxygen-bridged binuclear Fe species. The turnover frequency (TOF) for N_2O decomposition under dry and wet conditions has been confirmed assuming that Fe-ZSM-5-SSIE samples with Fe/Al = 0.20 and Fe/Al = 0.65 only contain mononuclear and binuclear Fe species, respectively, as active reaction species on their surface. The high performance of Fe-ZSM-5-SSIE may be mainly due to the formation of the binuclear Fe species onto its surface during the preparation of the catalyst.

Keywords: N_2O decomposition; Fe-ZSM-5; EXAFS; Oxygen-bridged binuclear Fe

1. Introduction

Fe-exchanged ZSM-5 is a potentially useful catalyst for a variety of chemical reactions such as the partial oxidation of hydrocarbons, $deNO_x$ by hydrocarbon, N_2O decomposition, etc. [1–13]. Fe-ZSM-5 containing a low iron loading or isomorphously substituted Fe has been recognized to be effective for the partial oxidation of benzene to phenol and of methane to methanol with N_2O as an oxidant of the related reaction [1–3]. Panov et al. [4] found that a particular state of adsorbed oxygen, called α-oxygen, is important for a partial oxidation reaction. Over-exchanged Fe-ZSM-5 catalysts have revealed high performance of catalytic activity and stability for selective catalytic reduction (SCR) of NO by hydrocarbons in the presence of a large excess of oxygen and water vapor [5,6], and for the decomposition of nitrous oxide (N_2O) to N_2 and O_2 within the temperature range above 300 °C [7–9]. Recently, Fe-ZSM-5 catalysts modified by steam-activation, alkaline treatment or Ru addition have been also suggested for the high performance of N_2O decomposition [10–13].

Feng and Hall [5,14] reported that a highly active Fe-ZSM-5 catalyst for the selective reduction of NO could be prepared by ion-exchange method with an aqueous solution of FeC_2O_4. However, their attempt to achieve the loadings of Fe onto a catalyst surface higher than about 70% ion-exchange level for the high $deNO_x$ performance, apparently failed [15]. As an alternative strategy, Chen and Sachtler suggested chemical vapor deposition (CVD) to obtain Fe-ZSM-5 catalyst with Fe/Al = 1 [6,16,17]. They insisted that the active reaction site for high $deNO_x$ performance was a binuclear oxygen-bridged complex, $[HO\text{-}Fe\text{-}O\text{-}Fe\text{-}OH]^{2+}$ formed on the catalyst surface during CVD [17], identified by H_2 and CO TPR, FTIR, EPR, and isotopic exchange with $^{18}O_2$ [16–18]. Marturano et al. [19] suggested that the distribution of iron on the surface of Fe-ZSM-5 strongly depended on the structure of the parent ZSM-5, confirmed by the formation of both diferric μ-oxo-bridged clusters and Fe_2O_3 particles during the ion-exchange procedure through EXAFS study. Battiston et al. also observed the existence of diferric oxo clusters on the catalyst surface by a preparation method employing CVD [20,21].

* Corresponding author. Tel.: +82 54 279 2264; fax: +82 54 279 8299.
E-mail address: isnam@postech.ac.kr (I.-S. Nam).

0926-3373/$ – see front matter © 2007 Elsevier B.V. All rights reserved.
doi:10.1016/j.apcatb.2007.09.020

Lobree and Bell [22] prepared Fe-ZSM-5 catalyst via a solid state ion-exchange method similar to that previously described by Chen et al. [16], and they proposed that Fe^{3+} cations were exchanged with the protons of Brønsted acid sites in a one-to-one basis when Fe/Al < 0.56. Fe exists in the form of dispersed cation such as $Fe(OH)_2^+$, $Fe(OH)^+$, and FeO^+, while small FeO_x particles appear to form on the surface of the catalyst containing higher Fe/Al ratio. Choi et al. [23] reported that the structure of Fe complexes on the surface of Fe-ZSM-5 was anticipated as either $Z^-[Fe(O)_2]^+$, or $Z^-[Fe(OH)_2]^+$, where Z^- represents the charge exchange site in the zeolite. It had been based upon the fact that the second RSF peak of the Fourier transformed EXAFS spectra originated from Fe–Al backscattering, not from Fe–Fe backscattering by Fourier analyses and EXAFS least squares fits for Fe-ZSM-5 catalyst prepared by solid state ion-exchange method. However, Pirngruber et al. [24] and Heijboer [25] clearly showed that the method by Choi et al. [23] for fitting EXAFS data to characterize Fe-ZSM-5 catalysts can hardly distinguish the backscattering by Fe from that by Al in Fe K-edge EXAFS spectra.

Yoshizawa et al. calculated the dissociation of nitrous oxide on a fully relaxed 3T cluster with a bare iron site $Z^-[Fe]^+$ in Fe-ZSM-5 [26]. Heyden et al. also comprehensively studied the reaction mechanism for the decomposition of N_2O on hydrated and dehydrated mononuclear iron sites over Fe-ZSM-5 using density functional theory [27]. Nobukawa et al. [28] also reported that only mononuclear Fe species existed over the catalyst containing low Fe content (Fe/Al = 0.1), whereas for Fe-ZSM-5 sample containing Fe/Al = 0.4, both mono- and binuclear Fe species coexisted. Hansen et al. [29] examined the reaction mechanism for the decomposition of nitrous oxide on hydroxylated and dehydroxylated binuclear oxygen bridged extra-framework iron sites on the surface of Fe-ZSM-5 by using density functional theory. They reported that a small amount of water existing in the feed gas stream was important for the decomposition activity of N_2O [29].

Other structures of Fe in Fe-ZSM-5 catalyst had been extensively investigated by Joyner and Stockenhuber [30,31], mainly using EXAFS technique. A variety of Fe states on the catalyst surface exist in forms of isolated metal ions, large oxide clusters and small oxygen-containing nanoclusters such as Fe_4O_4 and Fe_3O_4. They concluded that the state of the iron strongly depended on the preparation method [31]. The state and distribution of Fe on the surface of Fe-ZSM-5 have been still an issue in understanding the high performance of N_2O decomposition activity over the catalyst.

The purpose of this study is to systematically examine the effect of the preparation methods including solid state and wet ion exchanges with $FeCl_3$ and $Fe(NO_3)_3$, respectively, on the structure of Fe species formed on the surface of Fe-ZSM-5 catalysts confirmed by XRD, EXAFS, XANES, UV–vis, TPR, etc., and to optimize the content of Fe on the surface of ZSM-5 catalyst for the high performance of N_2O decomposition activity with respect to the method of catalyst preparation.

2. Experimental

2.1. Catalyst preparation

ZSM-5 (Si/Al = 27, H^+ type) obtained from Tosho Corp. has been employed as a parent catalyst for preparing a series of the Fe-based ZSM-5 catalysts in the present study. The catalyst was exchanged with a variety of concentrations of $Fe(NO_3)_3{\cdot}9H_2O$ (Aldrich, 98%) solution ranging from 0.001–0.01 M at room temperature for 12 h and pH 5–6. pH control was performed by adding ammonia solution to avoid the precipitation of FeOOH and/or $Fe(OH)_3$ during the course of the ion-exchange. It was followed by drying at 110 °C for 12 h and calcining at 550 °C in air for 5 h. Fe-based ZSM-5 catalysts containing a variety of Fe loadings were obtained by controlling the concentration of $Fe(NO_3)_3{\cdot}9H_2O$ solution and designated as Fe-ZSM-5-WIE-*x* in the present work, where *x* represents the Fe/Al ratio.

Another type of Fe-based ZSM-5 catalyst was prepared via a solid state ion-exchange method similar to that described by Lobree et al. [22]. The ZSM-5 was first calcined at 500 °C in a U type reactor, transferred to a glove box without contacting air and mechanically mixed with the appropriate amount of $FeCl_3$ required for the desired Fe-exchange level. While still in the glove box, this mixture was placed into a sealed reactor. The reactor was then removed from the glove box and placed on a furnace. A flow of He was passed through the reactor as it was heated at a rate of 1 °C/min to 310 °C, the sublimation temperature of $FeCl_3$. Upon the temperature reaching 310 °C, the reactor was held at this temperature for 4 h. The sample was then cooled to room temperature, removed from the reactor, and washed with deionized water until the precipitation of AgCl was not detected upon the addition of 1N $AgNO_3$ solution to the residual water. Finally, it was dried in an oven overnight at 110 °C. The catalyst sample was designated as Fe-ZSM-5-SSIE-*x*, where *x* is the Fe/Al ratio. The chemical compositions of the catalysts prepared in the present study were analyzed by inductive coupled plasma analyzer (ICP). The detailed physicochemical properties of the catalysts prepared in the present study are listed in Table 1.

2.2. Catalytic reactor system

The activity for the Fe-ZSM-5-WIE and -SSIE catalysts for N_2O decomposition was examined in a fixed-bed flow reactor, typically containing 0.5 g of the catalyst which was sieved into a mesh size of 20/30 in order to minimize the mass transfer limitations of the catalyst. Prior to the activity evaluation, the

Table 1
Chemical compositions of the catalysts prepared in the present study

Catalyst	Fe/Al	Fe (wt.%)	Catalyst	Fe/Al	Fe (wt.%)
SSIE 0.03	0.03	0.10	WIE 0.04	0.04	0.11
SSIE 0.20	0.20	0.61	WIE 0.15	0.15	0.45
SSIE 0.49	0.49	1.48	WIE 0.46	0.46	1.41
SSIE 0.65	0.65	1.96	WIE 0.67	0.67	2.02
SSIE 0.86	0.86	2.62	WIE 0.74	0.74	2.25
SSIE 0.95	0.95	2.89	WIE 1.04	1.04	3.17

catalyst was pretreated in situ with a total flow of 700 cc/min containing 79% He and 21% O_2 at 600 °C for 2 h, and then cooled to room temperature. A gas mixture consisting of 1000 ppm N_2O, 4% O_2, and with or without 10% H_2O in He balance was fed to the reactor system through Brooks mass flow controllers (Model 5850E). A total flow rate of 700 cc/min was mainly employed for the catalyst activity test, corresponding to GHSV = 42,000 h^{-1}. The concentration of feed and product streams was analyzed by using an on-line gas chromatograph (Hewlett Packard 5890 Series II) with a TCD detector. The conversions of the reactants are defined as follows:

$$\text{Conversion of } N_2O \text{ into } N_2(\%) = \frac{[N_2]_{\text{output}}}{[N_2O]_{\text{initial}}} \times 100(\%)$$

2.3. Catalyst characterization

Powder XRD patterns for the catalysts prepared in the present study were observed by using an M18XHF X-ray diffractometer with Ni-filtered Cu Ka radiation (λ ∼ 1.54184°). UV–vis reflection spectra were recorded at ambient temperature on a Shimadzu UV-2501PC Ultraviolet-visible (UV–vis) spectrometer equipped with an integration sphere ($BaSO_4$ was used as a reference). The samples were ground into the powder forms and treated at 500 °C in air for 1 h, and then immediately employed for UV–vis test to avoid the exposure to ambient atmosphere, particularly H_2O.

Temperature-programmed reduction in H_2 (H_2 TPR) was performed. The samples were pretreated at 500 °C for 2 h in flowing 21% O_2 in N_2 balance and then cooled to room temperature in N_2. After flushing 1% H_2 in N_2 at room temperature for 30 min, the catalyst was heated to 800 °C at 10 °C/min under flowing 1% H_2 in N_2. Water formed during the reduction of Fe was removed by an ice trap located downstream of the reactor and ahead of the TCD of GC.

X-ray absorption fine structure (XAFS) spectroscopic measurements were performed with synchrotron radiation by using the EXAFS facility installed at the beam line 3C1 in the Pohang accelerator laboratory. The ring was operated at 2.5 GeV and with 200 mA electron current and 1% coupling. The spectra were measured with an Si(1 1 1) channel-cut monochromator, whose energy was calibrated with the K-edge position of an Fe foil at 7112 eV. The samples were ground into the powder forms and treated at 500 °C in flowing pure He for 1 h, and put between two pieces of kapton tape, and then sealed in the glove box to avoid a re-exposure to ambient atmosphere. All the data were recorded in a transmission mode at room temperature, and Fe foil, FeO and α-Fe_2O_3 were employed as a reference compound. For Fe-ZSM-5 samples containing a content of Fe below 1 wt.%, EXAFS spectra were not relevant to be analyzed by the weak signal-to-noise ratio of their spectra, simply due to the limitation of the beam line 3C1 in the Pohang accelerator laboratory.

The data analyses for EXAFS were carried out by a standard procedure [32,33]. The inherent background in the data was removed by fitting a polynomial to the edge region and then extrapolated through the entire spectrum from which it was subtracted. The resulting spectra, $\mu(E)$, were normalized to an edge jump of unity for comparing the X-ray absorption near edge structure (XANES) directly with one another. The extended X-ray absorption fine structure (EXAFS) function, $\chi(E)$, was obtained from $\chi(E) = \{\mu(E) - \mu_0(E)\}/\mu_0(E)$ [32]. The resulting EXAFS spectra were k^2-weighted to compensate for the attenuation of EXAFS amplitude at high k and then Fourier transformed in the range of 2.5 $Å^{-1} \leq k \leq 11$ $Å^{-1}$ for Fe-ZSM-5-SSIE catalysts and 2.5 $Å^{-1} \leq k \leq 14$ $Å^{-1}$ for Fe-ZSM-5-WIE catalysts with a Hanning function. In order to determine the structural parameters, a nonlinear least square curve fitting was performed in the range of $R \leq \sim 3$ Å corresponding to the distance to the edge-shared Fe in the Fourier transformed (FT) spectra, by using the UWXAFS code according to the following EXAFS formula [34].

$$\chi(k) = -S_o^2 \sum_i \frac{N_i}{kR_i^2} F_i(k) \exp\{-2\sigma_i^2 k^2\} \exp\left\{\frac{-2R_i}{\lambda(k)}\right\} \times \sin\{2kR_i + \phi_i(k)\}$$

The backscattering amplitude, $F_i(k)$, the total phase shift, $\phi_i(k)$, and the photoelectron mean free path, $\lambda(k)$, have been theoretically calculated for all scattering paths including multiple ones by a curved wave *ab initio* EXAFS code FEFF8 [35].

3. Results and discussion

3.1. Effect of the preparation method for Fe-ZSM-5 catalysts on the decomposition activity of N_2O

N_2O decomposition over a series of Fe-ZSM-5-WIE and -SSIE catalysts was conducted within the reaction temperature range from 300 °C to 550 °C under the feed gas stream with or without 10% water, and their activity was examined with respect to the Fe content of the catalysts and the preparation method as shown in Fig. 1. Fe-ZSM-5-SSIE catalysts generally reveal higher N_2O decomposition activity than Fe-ZSM-5-WIE catalysts if Fe/Al > 0.2, and the highest activity of the Fe-ZSM-5-SSIE catalysts reaches to ca. 80% at a reaction temperature of 500 °C. The activity of Fe-ZSM-5 catalysts showed a typical monotonic pattern with respect to the reaction temperature [7,36–39], and for the Fe-ZSM-5-WIE, the N_2O decomposition activity under wet condition becomes considerably lower than that under dry condition as shown in Fig. 1(A) and (B). The result may be mainly attributed to the formation of the dehydroxylated and hydroxylated Fe species on the catalyst surface with respect to water in the feed gas stream [29]. The Fe-ZSM-5-SSIE catalysts with Fe/Al > 0.49 exhibit a light-off activity profile commonly observed for automotive catalyst, regardless of the presence of water in the feed, and their activities have reached to 80% conversion of N_2O to N_2 at reaction temperatures up to 550 °C, as depicted in Fig. 1(C) and (D). A serious water inhibition for the N_2O decomposition over Fe-ZSM-5-WIE and -SSIE catalysts prepared in the present

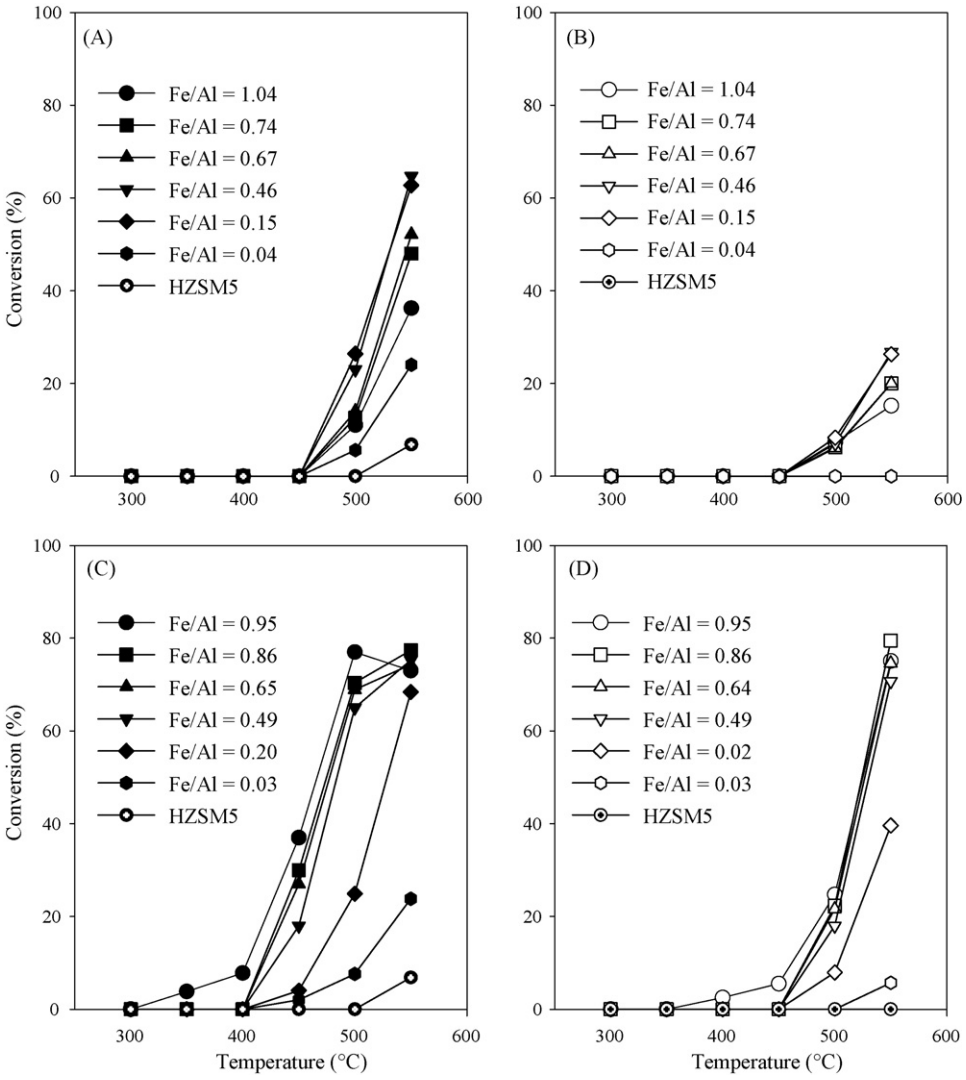

Fig. 1. N_2O decomposition activity over Fe-ZSM-5-WIE and -SSIE catalysts: Fe-ZSM-5-WIEs under (A) dry and (B) wet feed gas streams, and Fe-ZSM-5-SSIEs under (C) dry and (D) wet feed gas streams. (The gas composition is 1000 ppm N_2O and 4% O_2 with/without 10% H_2O in He balance.)

study has been observed that brings a shift of activity profile to a high temperature region by 50 °C.

Fig. 2 specifically illustrates the effect of the preparation method on N_2O decomposition activity with respect to the content of Fe over Fe-ZSM-5 catalysts. The general trend of the decomposition activity over a series of Fe-ZSM-5-SSIE catalysts increases to 80% of the conversion when Fe/Al $\geq$ 0.2 and levels off as Fe/Al ratio increases, regardless of the presence of water in the feed gas stream. However, the activity trend over Fe-ZSM-5-WIE catalysts is apparently inferior to that over Fe-ZSM-5-SSIE catalysts, probably due to the formation of Fe_2O_3 particle on the surface of Fe-ZSM-5-WIE catalysts during the course of the preparation [40]. Under wet condition at 500 °C, N_2O decomposition activity significantly decreased as shown in Fig. 2, compared to that at 550 °C, which may be due to the variation of the state of Fe species, dehydroxylated and hydroxylated on the catalyst surface proposed by Hansen et al. [29]. It should be noted that similar activity was achieved without water in the feed, particularly when Fe/Al $<$ 0.2, regardless of the preparation methods.

3.2. Characterization of Fe species formed in the framework of Fe-ZSM-5 prepared by WIE and SSIE

Fig. 3 shows the typical powder XRD patterns for the series of the Fe-ZSM-5 catalysts prepared by WIE and SSIE methods. Their powder XRD patterns well agree with that of H-ZSM-5, except for the slight alterations in the relative intensities of X-ray peaks and their positions due to the loadings of Fe on the catalyst surface. It simply reflects that Fe loading hardly affects the framework of ZSM-5 type zeolite. However, a new broad XRD peak for Fe-ZSM-5-WIE catalysts containing Fe/Al $>$ 0.2 can be observed at 2θ of ca. 33° indicating the formation of α-Fe_2O_3 on the catalyst surface, while for Fe-ZSM-5-SSIE catalysts no patterns for confirming the formation of α-Fe_2O_3, γ-Fe_2O_3, FeO, etc., have been observed. It may indicate that the formation of Fe_2O_3 on the catalyst surface critically depends on the preparation method of Fe-ZSM-5 catalyst and Fe loading. Such an aggregation of Fe could definitely cause a decrease of N_2O decomposition activity, particularly over Fe-ZSM-5-WIE catalysts containing Fe/Al $>$ 0.4.

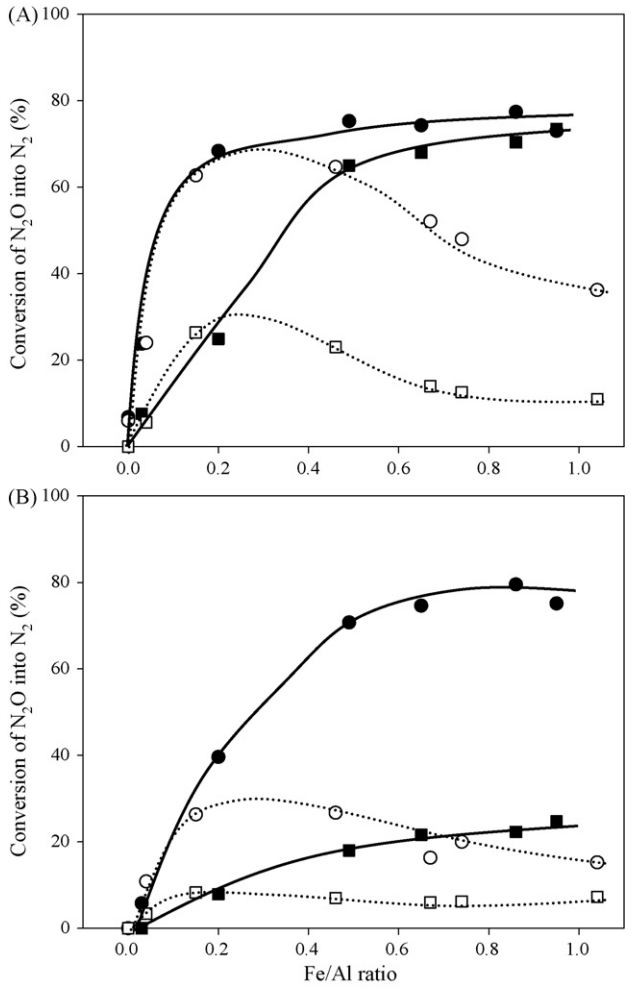

Fig. 2. N_2O decomposition activity of Fe-ZSM-5 catalysts with respect to Fe/Al ratios under (A) dry and (B) wet conditions: Fe-ZSM-5-SSIEs at 550 °C (●) and 500 °C (■), and Fe-ZSM-5-WIEs at 550 °C (○) and 500 °C (□).

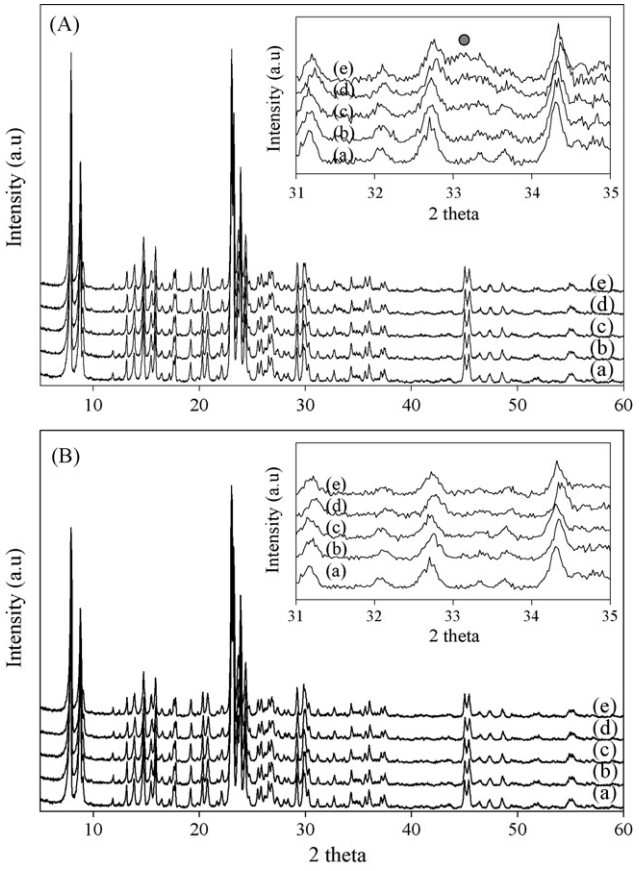

Fig. 3. XRD patterns of (A) Fe-ZSM-5-WIE catalysts when (a) without Fe, and Fe/Al = (b) 0.15, (c) 0.46, (d) 0.67 and (e) 1.04, and (B) Fe-ZSM-5-SSIE catalysts when (a) without Fe, and Fe/Al = (b) 0.20, (c) 0.49, (d) 0.86 and (e) 0.95.

H_2 TPR experiments were conducted over Fe-ZSM-5-WIE and -SSIE samples, as shown in Fig. 4. TPR spectra for the catalysts, except Fe-ZSM-5-WIE-1.04, show a similar pattern containing a major peak at ca. 430 °C, regardless of the preparation method. Note that a small peak between 30 °C and 100 °C may be an artifact, probably due to desorption of residual H_2O or N_2 remaining in the TPR system even after purge. The desorption temperature and shape of the main peak observed for the Fe-ZSM-5 catalysts are quite relevant to the first peak of the TPR pattern over a reference, Fe_2O_3 due to the transformation of Fe^{3+} to Fe^{2+}. The amount of H_2 consumption based upon the integrated area of the main peak from 200 °C to 600 °C increases as the Fe loading of the catalysts increases. Besides Fe-ZSM-5-SSIE-0.20, and -WIE-0.15 catalysts, the H_2/Fe ratio of the catalysts calculated from the integrated area and Fe loading is nearly identical, ca. 0.5, regardless of the catalysts, as listed in Table 2. It may simply be that almost all of the trivalent irons located at the cation exchange sites of zeolite structure can be reduced to Fe^{2+} [16]. Most of the Fe formed on the catalyst samples exists in the form of Fe^{3+} confirmed by their XANES spectra to be discussed later. Based upon the theoretical calculation of the H_2/Fe consumption over a variety of iron oxide species possibly formed on the catalyst surface as shown in Fig. 5, H_2/Fe = 0.5 might be attributed to the reduction of oxygen-bridged binuclear Fe species or of the mixture of mononuclear Fe species and α-Fe_2O_3 particles. Mononuclear iron oxide species is expected to exist in form of mesomeric Fe [Fe(III)-$O^{\bullet -}$, Fe(III) radical anion ↔ Fe(IV) = O, Fe(IV) oxo mesomer] [41], which can be hardly identified in the present study.

The pattern of TPR spectra over both Fe-ZSM-5-WIE-0.15 and -SSIE-0.20 catalysts is quite similar, particularly the major peak at ca. 430 °C, which may be related to the trend of N_2O decomposition activity as reported in Fig. 2. A similar structure of the active Fe site formed on the catalyst surface may be anticipated when Fe/Al < 0.2, regardless of the preparation method of Fe-ZSM-5 catalysts. The general trends of TPR profiles for Fe-ZSM-5-SSIE catalysts are similar, regardless of the Fe/Al ratios of the catalysts, except that the development of a shoulder peak at ca. 600 °C, and a temperature shift of the main peak from 460 °C to 410 °C has been also observed as Fe/Al increases, and the reduction peak at around 430 °C seems to be the major one within the temperature range from 200 °C to 600 °C. However, the shape and location of the TPR profiles over Fe-ZSM-5-WIE catalysts change considerably as the Fe content increases.

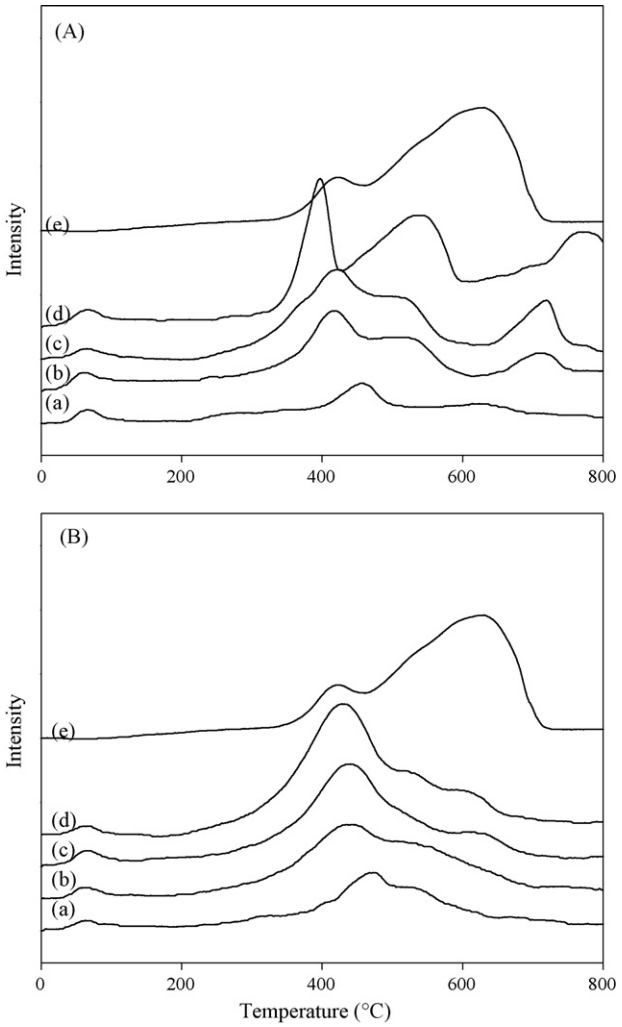

Fig. 4. H_2-TPR profiles for (A) Fe-ZSM-5-WIE catalysts when Fe/Al = (a) 0.15, (b) 0.46, (c) 0.67, (d) 1.04 and (e) Fe_2O_3 as a reference and (B) Fe-ZSM-5-SSIE catalysts when Fe/Al = (a) 0.20, (b) 0.49, (c) 0.86, (d) 0.95 and (e) Fe_2O_3.

A new H_2 consumption peak for Fe-ZSM-5-WIE containing Fe/Al $\geq$ 0.46 has been developed in the temperature range of the desorption peak higher than 700 °C. The pattern over Fe-ZSM-5-WIE-1.04, however, is quite distinctive compared to those over the rest of the catalyst samples. The reduction peak at high temperature may be attributed to the transformation of iron oxide particles to metallic irons on the catalyst surface

Table 2
H_2/Fe consumption ratios obtained from TPR spectra for the catalysts employed in the present study

Catalyst	Fe/Al	H_2/Fe	Catalyst	Fe/Al	H_2/Fe
SSIE 0.20	0.20	1.15[a] (1.25)[b]	WIE 0.15	0.15	1.08 (1.30)
SSIE 0.49	0.49	0.70 (0.75)	WIE 0.46	0.46	0.63 (0.77)
SSIE 0.65	0.65	0.61 (0.68)	WIE 0.67	0.67	0.45 (0.55)
SSIE 0.86	0.86	0.5 (0.53)	WIE 0.74	0.74	
SSIE 0.95	0.95	0.57 (0.60)	WIE 1.04	1.04	0.55 (0.79)

[a] The consumption ratio (H_2/Fe) obtained from TPR spectra ranged from 200 °C to 600 °C for the given catalysts.
[b] The consumption ratio (H_2/Fe) obtained from TPR spectra ranged from 200 °C to 800 °C for the given catalysts.

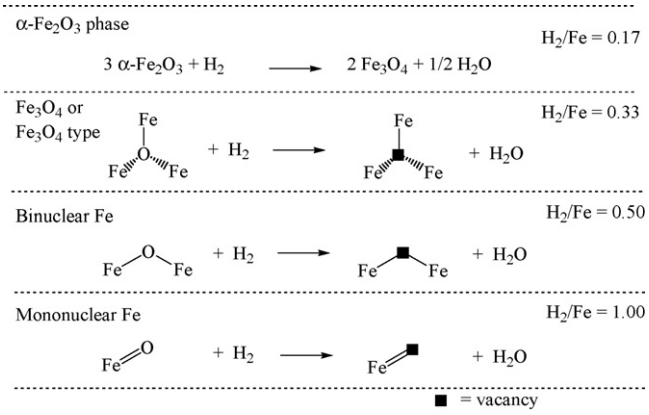

Fig. 5. H_2/Fe ratios based upon theoretical consumption of hydrogen for the reduction of Fe(III) to Fe(II) in (a) α-Fe_2O_3 phase, (b) Fe_3O_4 or Fe_4O_4 cluster species, (c) binuclear iron oxide species and (d) mononuclear iron oxide.

[16,17,42]. The H_2 TPR results may reveal that Fe-ZSM-5 catalysts containing Fe/Al $\leq$ 0.2 include mononuclear iron oxides on their surface as a major species, regardless of the preparation method. When Fe/Al > 0.4, the Fe-ZSM-5-SSIE

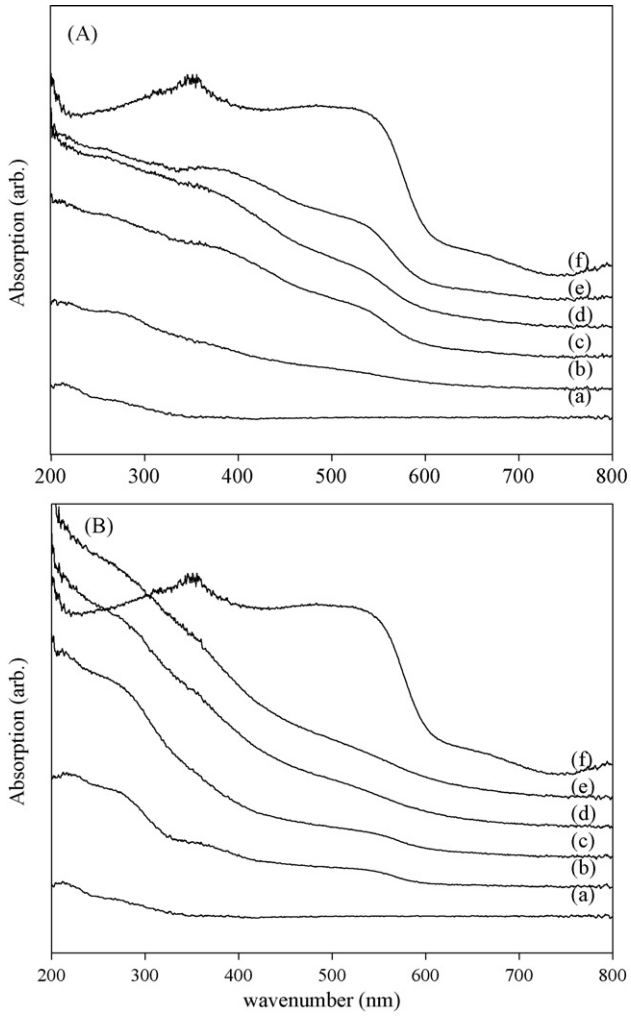

Fig. 6. UV–vis spectra of (A) Fe-ZSM-5-WIEs when (a) without Fe, Fe/Al = (b) 0.15, (c) 0.46, (d) 0.74, (e) 1.04 and (f) Fe_2O_3 and (B) Fe-ZSM-5-SSIEs when (a) without Fe, Fe/Al = (b) 0.20, (c) 0.49, (d) 0.86, (e) 0.95 and (f) Fe_2O_3.

and -WIE catalysts may contain oxygen-bridged binuclear iron species, and mononuclear iron oxides and Fe_2O_3 particles on their surfaces, respectively. This will be further discussed later.

Electronic spectroscopy in the UV–vis region may provide useful information on the electronic state and coordination of Fe species on the surface of zeolites. In general, UV–vis spectrum can be classified into two categories [43–46]: the first region may be in the range of wave number from 200 nm to 350 nm, where strong absorption peaks due to ligand-to-metal charge transfer can be observed [43,44], and another region from 350 nm to 600 nm, where weak peaks related to d–d transition of the transition metal ion can be identified [44–46].

The UV-spectra of Fe-ZSM-5-WIE and -SSIE catalysts have been examined in the wavelength range of 200–800 nm, as depicted in Fig. 6. For a comparative study, the absorption spectrum of the reference sample, α-Fe_2O_3, revealing octahedral coordination has been also observed. Fe-ZSM-5 catalysts exhibited four distinctive absorption bands centered at about 224 nm, 275 nm, 360 nm and 550 nm. The former two peaks at 224 nm and 275 nm can be assigned to the ligand-to-metal charge-transfer (LMCT) transitions of Fe^{3+} ion containing octahedral symmetry [44]. Since the $AgNO_3$ test for the preparation of the SSIE catalysts reveals that the concentration of chlorine in the catalyst sample was negligible, these absorptions are mainly attributed to O → Fe LMCT transitions in the Fe-ZSM-5 catalysts.

Table 3
Characteristic peak positions of Fe K-edge for the Fe-ZSM-5-WIE and -SSIE catalysts and a reference, α-Fe_2O_3

Sample	Fe/Al	Peak I[a]	Peak II[b]	Peak III	Peak IV
α-Fe_2O_3		7113.8	7124.0	7127.3	7133.9
Fe-ZSM-5-WIE	0.15	7113.9		7127.1	
	0.46	7113.7	7123.9	7127.9	7132.8
	0.74	7113.7	7124.0	7127.9	7133.1
	1.04	7113.8	7124.0	7127.9	7133.1
Fe-ZSM-5-SSIE	0.20	7113.2	7123.2	7126.5	7136.3
	0.49	7113.2	7123.2	7126.5	7136.0
	0.86	7113.2	7123.0	7127.0	7136.3
	0.95	7113.3	7123.0	7126.8	7136.9

[a] Corresponding to the pre-edge energy (eV).
[b] Eo energy (eV) i.e., edge energy of Fe K-edge for the samples.

The broad peaks at ca. 360 nm and 550 nm in UV–vis spectra of Fe-ZSM-5 catalysts are mainly due to the d–d transition of Fe^{3+} ion similar to those of Fe_2O_3. These peaks can be assigned to the transition of $^6S \rightarrow {}^4G$ and $^6S \rightarrow {}^4D$, respectively, based upon the Fe^{3+} ion existing in a form of high spin d^5 configuration containing octahedral symmetry [45]. It may also be indicative of the presence of Fe^{3+} ions on the catalyst surface in an aggregated form such as iron hydroxide or/and oxide clusters revealing similar peak positions in the spectrum of Fe_2O_3 employed as a reference sample [46]. The relative intensities of the LMCT bands over Fe-ZSM-5-WIE catalysts are considerably lower than those

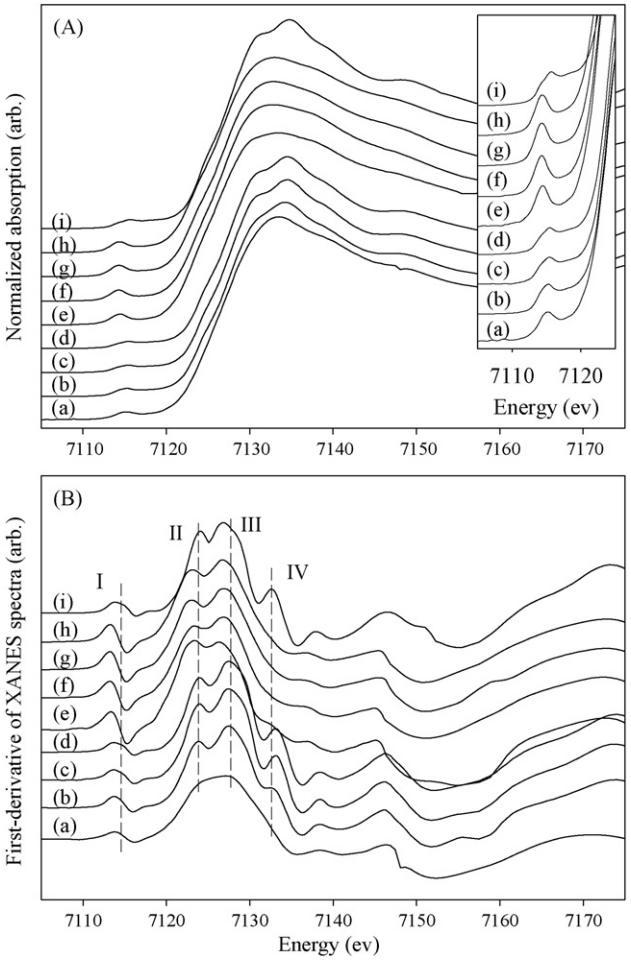

Fig. 7. (A) Normalized Fe K-edge XANES spectra and (B) their first-derivatives for Fe-ZSM-5-WIEs when Fe/Al = (a) 0.15, (b) 0.46, (c) 0.74 and (d) 1.04, and for Fe-ZSM-5-SSIEs when Fe/Al = (e) 0.20, (f) 0.49, (g) 0.86, (h) 0.95 and (i) Fe_2O_3 as a reference.

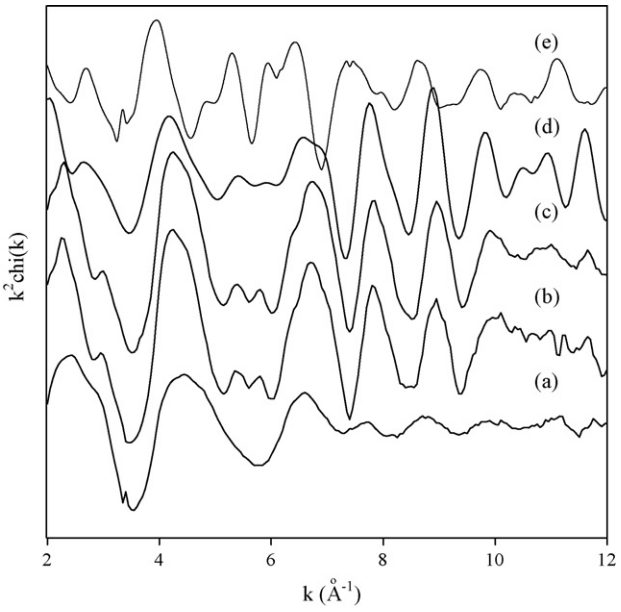

Fig. 8. Experimental Fe K-edge k^2-weighted EXAFS data for (a) Fe-ZSM-5-SSIE-0.86, (b) Fe-ZSM-5-WIE-0.67, (c) Fe_2O_3, (d) α-Fe_2O_3 calculated by *ab initio* EXAFS code FEFF8 and (e) FeO calculated by an *ab initio* EXAFS code FEFF8.

over Fe-ZSM-5-SSIE catalysts. However, the intensities of the d–d transition peaks at ca. 360 nm and 550 nm are substantially high. These results may be another key evidence for the formation of a significant amount of iron on the catalyst surface aggregating into Fe oxide clusters over Fe-ZSM-5-WIE catalysts. It is also quite consistent with the qualitative nature of the catalyst of which the color is dark reddish, similar to that of hematite (α-Fe_2O_3). These results will be further confirmed by XAFS.

3.3. Local structure of Fe ions on the surface of Fe-ZSM-5 catalysts

The shape and position of the Fe K-edge X-ray absorption near edge structure (XANES) provide information on the electronic structure and the local coordination geometry of the absorbing Fe atom [28,47–52]. Fig. 7(A) shows the XANES spectra for Fe-ZSM-5-WIE and -SSIE catalysts, which are quite typical for confirming the existence of the distorted octahedral and tetrahedral Fe^{3+} on the catalyst surface, respectively. In order to identify the peak position of the absorption edge (E_o) defined as the maximum of the first derivative of the XANES spectrum, the first derivatives of the spectra over Fe-ZSM-5 catalysts along with the references including Fe_2O_3 have been also calculated and their results are basically identical, as shown in Fig. 7(B).

A pre-edge peak (I) for Fe-ZSM-5-WIE catalysts has been commonly observed at ca. 7113.8 eV. Their intensities, however, are weaker than that of Fe-ZSM-5-SSIE catalyst at ca. 7113.2 eV, mainly due to the quadruple transition from 1s to 3d of Fe^{3+} containing octahedral, tetrahedral and/or square pyramidal symmetry [47,50]. Three kinds of sub-patterns for the pre-edge K-edge XANES spectrum over Fe-ZSM-5-WIE catalysts also observed over Fe_2O_3, a reference sample, disappear as shown in the inset of Fig. 7(A). It is generally recognized that the sub-patterns can be specifically assigned to the transition of 1s to t_{2g}, e_g, and the higher conduction sub-bands when a high spin ground-state Fe^{3+} ($3d^5$) ion is occupied by an octahedral crystal field [47,49–52]. However, the pre-edge peak obtained from tetrahedral Fe ion reveals higher absorption intensity than that from centro-symmetric Fe species in a octahedral form due to dipole-allowed state caused by the loss of inversion symmetry at the iron site, which corresponds

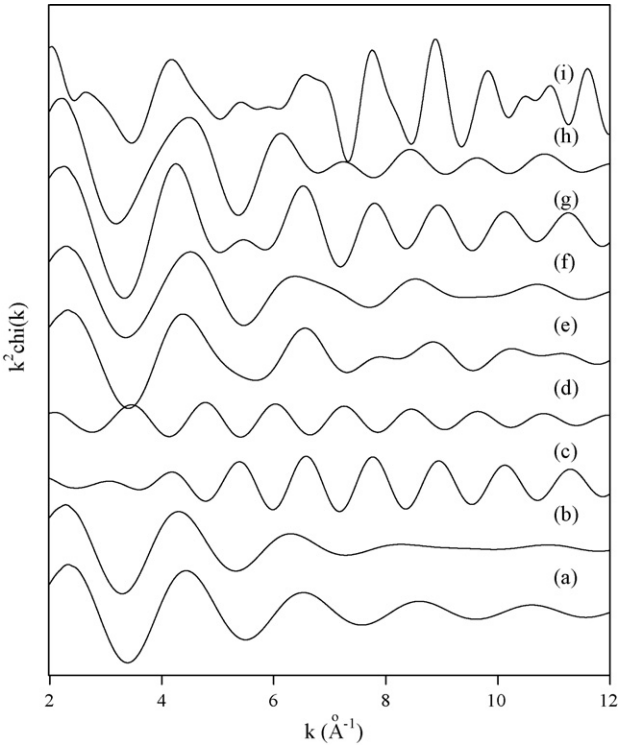

Fig. 9. Theoretical Fe K-edge k^2-weighted EXAFS spectra for (a–h) the combinations of the backscattering of Fe–O(I), Fe–O(II), Fe–Fe and Fe–Al pairs: (a) 3× Fe–O(I) and 1× Fe–O(II), (b) 3× Fe–O(I) and 3× Fe–O(II), (c) 3× Fe–Fe, (d) 3× Fe–Al, (e) 3× Fe–O(I), 1× Fe–O(II) and 1× Fe–Fe, (f) 3× Fe–O(I), 1× Fe–O(II) and 1× Fe–Al, (g) 3× Fe–O(I), 3× Fe–O(II) and 3× Fe–Fe, (h) 3× Fe–O(I), 3× Fe–O(II) and 3× Fe–Fe and for (i) α-Fe_2O_3 as a reference sample. The backscattering spectra of Fe–O(I) [R_{eff} = 1.9457 Å], Fe–O(I) [R_{eff} = 2.1162 Å], Fe–Fe [R_{eff} = 2.9710 Å], and Fe–Al [R_{eff} = 2.9710 Å] have been calculated by an *ab initio* EXAFS code FEFF8 on the basis of the crystalline structure of α-Fe_2O_3.

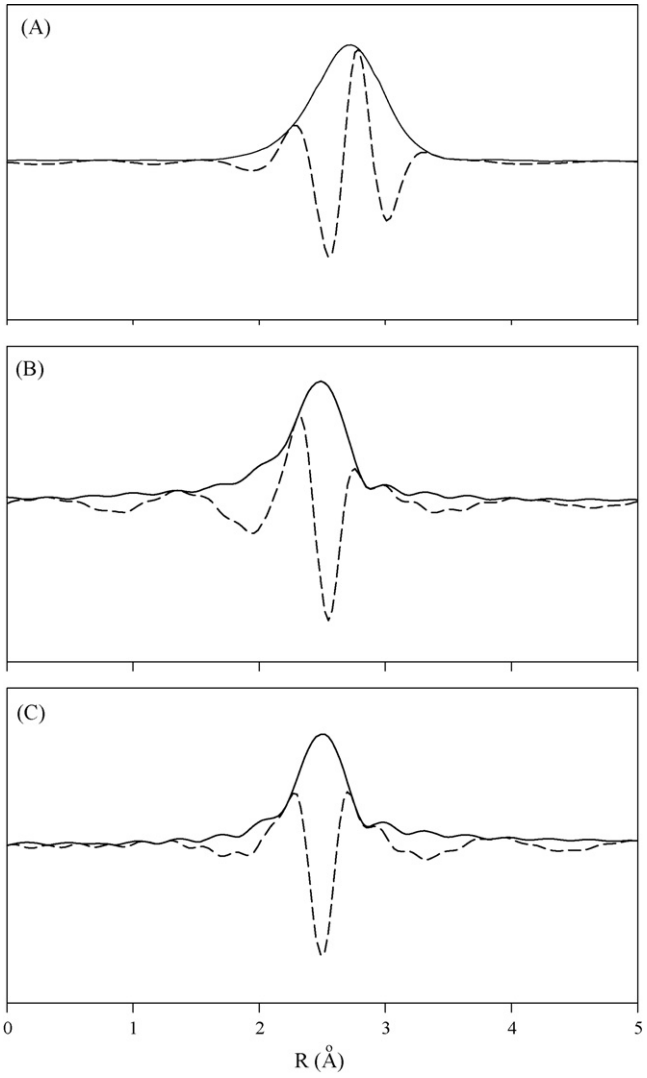

Fig. 10. Theoretical Fe K-edge k^2-weighted Fourier transformed EXAFS spectra for the backscattering of (A) Fe–Fe, (B) Fe–Al and (C) Fe–Si pairs.

to the mixing of the 4p and 3d metal orbitals based upon the electric-quadrupole coupling mechanism [46,49–52].

The absorption edge (II) over the spectra of Fe-ZSM-5 appears at ca. 7123 eV, as summarized in Table 3, mainly due to the dipole-allowed transition of 3d–4p mixing orbital. It simply indicates that the Fe ions in the framework of Fe-ZSM-5 catalyst prepared exist in the form of trivalent Fe [23,30,50]. The intensity of the absorption edge of Fe-ZSM-5-WIE catalysts seems to be higher than that of Fe-ZSM-5-SSIE catalysts, and to be similar to that of α-Fe_2O_3, a reference sample. And two other peaks, (III) and (IV), appear at ca. 7127 eV and 7133–7137 eV by the transition of Fe ion from 1s to 4p orbital or d–p mixing between metal atom and ligands through bonding and multiple scattering [46,47,50]. These peaks in the Fe K-edge of the Fe-ZSM-5-WIE catalysts are also similar to that of the characteristic peaks for Fe_2O_3, besides that of Fe-ZSM-5-WIE-0.15. In particular, the peak (IV) of ca. 7135 eV, which may be attributed to multiple scattering by relatively heavy backscatters including Fe [46,47,50], disappeared for Fe-ZSM-5-SSIE catalysts. In addition, the Fe-ZSM-5-WIE-0.15 catalyst exhibited a distinctive pattern in the identical energy region compared to the rest of the catalysts prepared by WIE. It can be anticipated that Fe ion on the surface of Fe-ZSM-5-WIE catalysts besides the catalyst containing Fe/Al = 0.15 may exist in the form of small Fe_2O_3-like particles. It is also quite consistent with the UV–vis results as discussed, and will be reconfirmed again by the analysis of their EXAFS spectra.

Extended X-ray absorption fine structure (EXAFS) spectroscopy has been recognized to be an effective tool for exploring

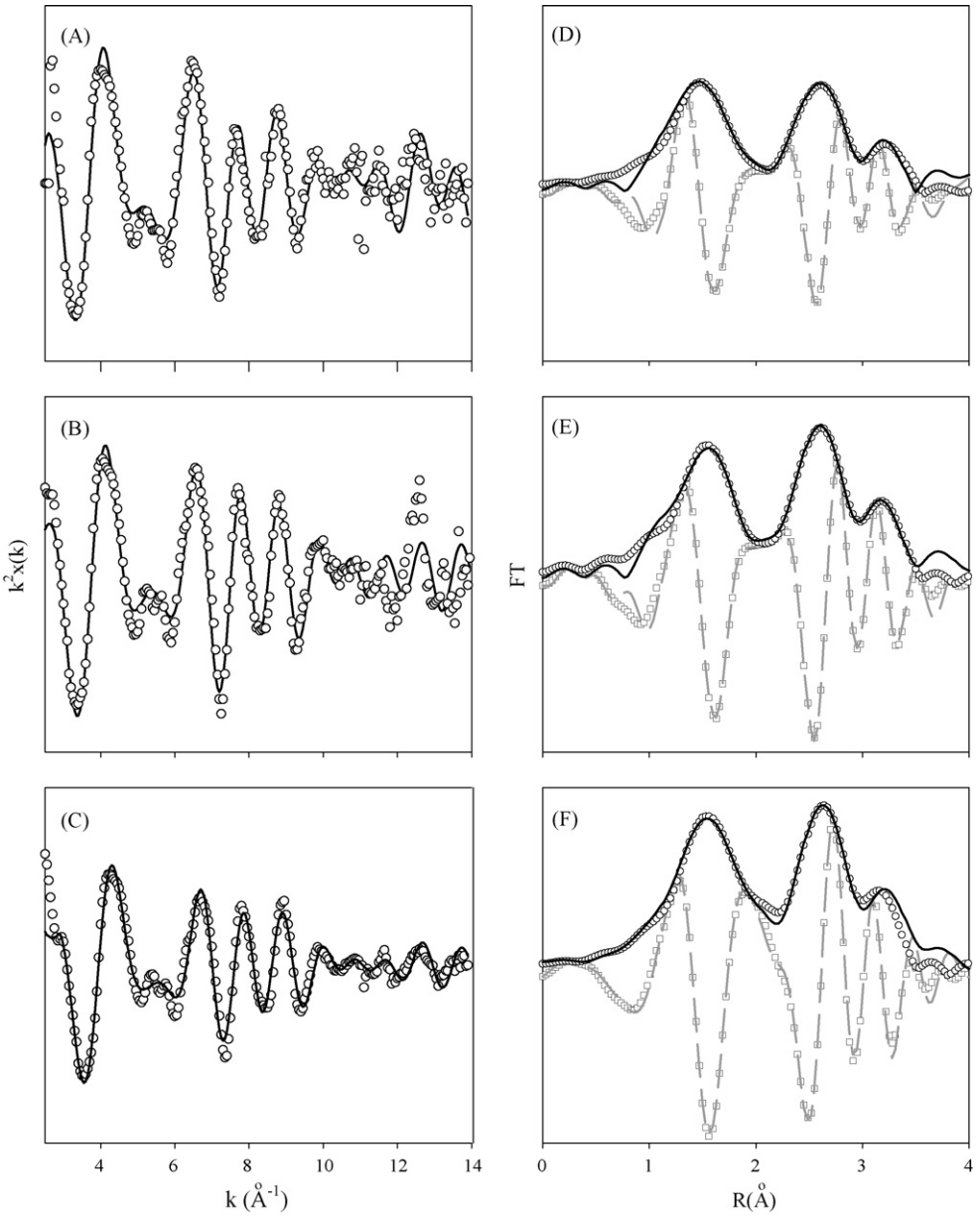

Fig. 11. Fe K-edge k^2-weighted EXAFS data (dotted) and best fits (solid) for Fe-ZSM-5-WIE catalysts with Fe/Al = (A) 0.46, (B) 0.74 and (C) 1.04, and their Fourier transformed data (dotted) and best fits (solid) for Fe-ZSM-5-WIE catalysts with Fe/Al = (D) 0.46, (E) 0.74 and (F) 1.04.

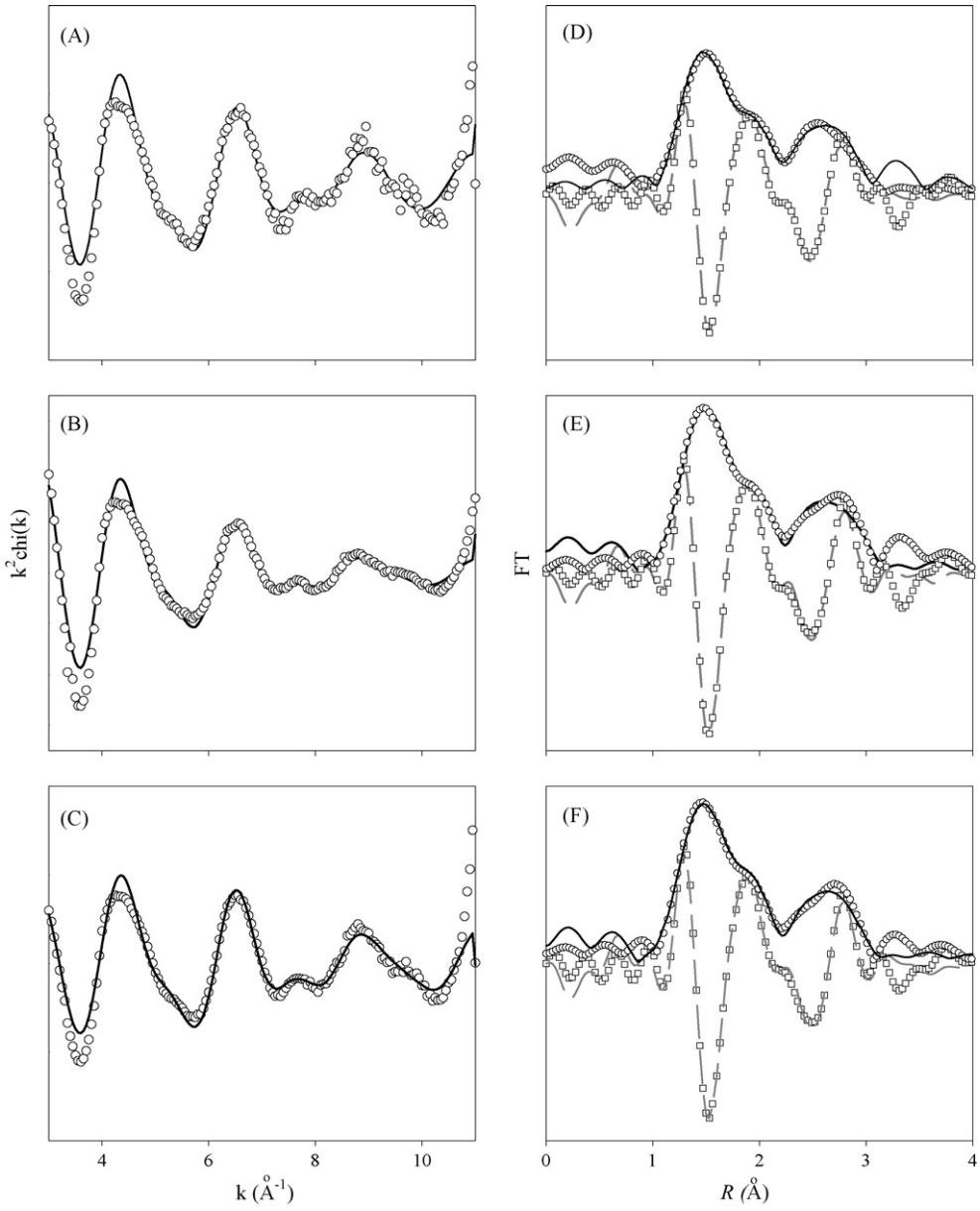

Fig. 12. Fe K-edge k^2-weighted EXAFS data (dotted) and best fits (solid) for Fe-ZSM-5-SSIE catalysts with Fe/Al = (A) 0.46, (B) 0.74 and (C) 1.04, and their Fourier Transformation data (dotted) and best fits (solid) for Fe-ZSM-5-SSIE catalysts with Fe/Al = (D) 0.46, (E) 0.74 and (F) 1.04.

interatomic distances and coordination numbers to examine the geometry of the reaction sites, since it is mainly due to the interaction between absorbing and nearly surrounding atoms [19–21,23–25,33,52–54].

The EXAFS spectra for the Fe-ZSM-5-WIE and -SSIE catalysts are similar to each other in a wide range of k compared to the spectra of α-Fe_2O_3, which are experimentally and theoretically obtained by an *ab initio* EXAFS code FEFF8 on the basis of the crystalline structure of α-Fe_2O_3 as shown in Fig. 8. However, the fine feature of EXAFS spectra over Fe-ZSM-5-SSIE catalysts is not particularly distinctive in the high value region of k except the amplitude of $k^2 \times \chi(k)$. To understand the characteristic patterns of $\chi(k)$ spectra for Fe-ZSM-5-SSIE catalysts and the reference, α-Fe_2O_3 in the k ranging from 4 $Å^{-1}$ to 6 $Å^{-1}$, the theoretical $\chi(k)$ spectra for the backscattering Fe–O(I) [R_{eff} = 1.9457 Å], Fe–O(II) [R_{eff} = 2.1162 Å], Fe–Fe [R_{eff} = 2.9710 Å], and Fe–Al [R_{eff} = 2.9710 Å] pairs, and their combinations based on the crystalline structure of α-Fe_2O_3 have been calculated by an *ab initio* EXAFS code FEFF8 as shown in Fig. 9. The theoretically calculated $\chi(k)$ spectrum for the combination of 3× Fe–O(I), 1× Fe–O(II), and 1× Fe–Fe pairs is quite similar to that of the Fe-ZSM-5-SSIE catalysts, not to the combination of 3× Fe–O(I), 1× Fe–O(II), and 1× Fe–Al pairs. The combined $\chi(k)$ spectrum of 3× Fe–O(I), 3× Fe–O(II), and 6× Fe–Fe pairs is relevant to that of Fe-ZSM-5-WIE catalysts.

To further identify the second neighbor at ca. 2.7 Å in the RSF spectra over the catalysts prepared, the theoretical backscatterings for Fe–Fe, Fe–Al and Fe–Si pairs have been examined by k^2-weighted Fourier transformation of the theoretical data of Fe K-edges with *ab initio* EXAFS code,

Table 4
EXAFS results of Fe-ZSM-5-WIE and -SSIE catalysts

	Shell	CN[a]	R (Å)	σ^{2b}	R^c
WIE 0.46	Fe–O1	3.0	1.92	0.0	0.028
	Fe–O2	3.5	2.04	0.6	
	Fe–Fe1	3.0	2.97	2.9	
	Fe–Fe2	3.5	3.38	3.2	
WIE 0.67	Fe–O1	2.7	1.97	2.9	0.014
	Fe–O2	3.1	2.09	5.5	
	Fe–Fe1	2.7	2.97	6.0	
	Fe–Fe2	3.1	3.39	2.0	
WIE 1.04	Fe–O1	3.6	1.94	3.7	0.015
	Fe–O2	3.6	2.09	5.5	
	Fe–Fe1	2.9	2.97	5.4	
	Fe–Fe2	3.6	3.34	2.0	
SSIE 0.49	Fe–O1	0.9	1.91	1.0	0.015
	Fe–O2	1.5	2.03	3.7	
	Fe–Fe	0.9	3.01	26.2	
SSIE 0.86	Fe–O1	1.4	1.89	1.5	0.013
	Fe–O2	2.3	2.01	4.2	
	Fe–Fe	0.9	3.05	19.9	
SSIE 0.95	Fe–O1	1.7	1.89	1.0	0.013
	Fe–O2	2.8	2.00	3.5	
	Fe–Fe	0.8	3.04	17.1	

[a] Coordination number.
[b] Debye–Waller factor ($\sigma^2 \times 10^{-3}$ Å^2).
[c] R-factor.

FEFF8 as presented in Fig. 10 [23,31] similar to that described by Choi et al. [23]. In general, the imaginary parts of the Fourier transformed data may be a characteristic for the absorber-backscatter pair, regardless of the distance between the absorber and the backscatter or the coordination number of the backscatter [23,33]. Therefore, by a comparison of the imaginary part of the RSF in the region of 2–3 Å to those of the theoretical backscatterings for Fe–Fe, Fe–Al or Fe–Si, the second shells obtained from the Fe-ZSM-5 catalysts prepared can be identified [23,33]. The imaginary part for Fe-ZSM-5 catalysts seems to be similar to that of Fe–Fe backscattering, not Fe–Al and Fe–Si, as clearly observed in Fig. 10. However, Pirngruber et al. [24] and Heijboer [25] have demonstrated that the backscatterings by Fe and Al can be hardly distinguished for characterizing the form of Fe species on the surface of Fe-ZSM-5 catalysts only with EXAFS analysis, which is quite consistent to the results by the interpretation of EXAFS discussed in the present study. In fact, the present work has integrated the experimental and theoretical results and observations by a variety of the catalyst characterization methods including, XRD, UV–vis, XAFS analysis, *ab initio* EXAFS calculation, and the amount of H_2 consumption by TPR employed to confirm the presence of Fe–O–Fe on the surface of Fe-ZSM-5 catalysts prepared.

These results may simply provide strong evidence that the first and second nearest neighboring peaks are mainly corresponding to Fe–O and edge-shared Fe–Fe scatterings, respectively, similar to those in α-Fe_2O_3. Therefore, the least square curve fitting of the first and second shells in the Fe K-edge k^2-weighted FT EXAFS spectra for the Fe-ZSM-5 catalysts has been performed on the basis of the Fe–O and edge-shared Fe–Fe backscatterings, theoretically calculated from the local structure of Fe based on crystalline α-Fe_2O_3 data by using an *ab initio* EXAFS code FEFF8.

Figs. 11 and 12 show the Fe K-edge k^2-weighted EXAFS spectra for Fe-ZSM-5-WIEs and -SSIEs, respectively, and a Fourier transformation (FT) of the spectra has been conducted in the range of 2.5 Å^{-1} ≤ k ≤ 11 Å^{-1} and 2.5 Å^{-1} ≤ k ≤ 14 Å^{-1} with a Hanning function. As observed in Figs. 11 and 12, the best fits of the EXAFS data for Fe-ZSM5 catalysts have been attained, and their parameters are summarized in Table 4. The neighboring shells in Fourier transformed Fe K-edge EXAFS spectra for the catalyst samples were found to be ca. 4× Fe–O and ca. 1× Fe–Fe for Fe-ZSM-5-SSIE, and ca. 6× Fe–O and 4–6× Fe–Fe for Fe-ZSM-5-WIE. It reveals that most of Fe species over Fe-ZSM-5-SSIE are well dispersed on the catalyst surface in a form of binuclear Fe species at the ion-exchange site of ZSM-5 catalyst, and Fe ions are aggregated into Fe_2O_3 in the form of particles on the external surface of Fe-ZSM-5-WIE catalysts. The binuclear Fe species can be regarded as a notable active reaction site for the high performance of N_2O decomposition over Fe-ZSM-5-SSIE catalyst, specifically containing a high amount of Fe on the catalyst surface.

The oxygen shells close to Fe–O1 (ca. 1.9 Å) and Fe–O2 (ca. 2.0 Å) over Fe-ZSM-5-SSIE catalysts can be assigned to an Fe–O–Fe (or Fe–O–Al) bridging oxygen atom or a terminal hydroxyl group [20,21]. For Fe-ZSM-5-WIE, the initial two close oxygen shells, Fe–O1 and Fe–O2, are similar to that of α-Fe_2O_3 lattice containing two Fe–O bonds of 1.96 Å and 2.08 Å in the distorted octahedral Fe sites, respectively, and two Fe shells, Fe–Fe1 and Fe–Fe2, can be also assigned to the edge-shared Fe–Fe and corner-shared Fe–Fe over α-Fe_2O_3.

Table 5
Major Fe species formed on the surface of Fe-ZSM-5 catalysts prepared

Fe/Al ratio	Fe/Al ≤ 0.2	Fe/Al > 0.2
Fe-ZSM-5-WIE catalysts		
Major Fe species	Mononuclear Fe species	Mononuclear Fe species and/or α-Fe_2O_3 or large iron oxides or binuclear Fe species
Method of analyses	TPR, theoretical H_2 consumption, UV–vis	TPR, XRD, theoretical H_2 consumption, XAFS, *ab initio* EXAFS calculation, pattern of imaginary part of RSF, UV–vis
Fe-ZSM-5-SSIE catalysts		
Major Fe species	Mononuclear Fe species	Binuclear Fe species
Method of analyses	TPR, theoretical H_2 consumption, UV–vis	TPR, theoretical H_2 consumption, XAFS, *ab initio* EXAFS calculation, pattern of imaginary part of RSF

3.4. Role of Fe species for the decomposition activity of N_2O

Based upon the integration of the experimental and theoretical results and observations confirmed in the present study, the major species of Fe formed on the surface of Fe-ZSM-5 catalysts in the present study can be anticipated with respect to the Fe contents and the preparation method of the catalysts, as also summarized in Table 5. Fe-ZSM-5-SSIE and WIE catalysts with low Fe loadings were found to contain mononuclear Fe species as the major species, which is confirmed by their TPR and UV–vis spectra. The decomposition activities of both catalysts are similar with respect to Fe content of the catalysts containing low Fe/Al ratio, regardless of the preparation method as depicted in Fig. 2. For Fe-ZSM-5-WIE catalysts with relatively high Fe/Al ratio (>0.2), the N_2O decomposition seems to be suppressed by the formation of Fe_2O_3 particles as observed by XRD and XAFS results. Fe-ZSM-5-SSIE catalysts with high Fe loading (Fe/Al > 0.2), the Fe species may be mainly existing in a form of binuclear Fe such as oxygen-bridged binuclear Fe complex, not larger multinuclear Fe clusters.

It can be also confirmed by the calculation of turnover frequency (TOF) of the present catalytic system by assuming that Fe-ZSM-5-SSIE samples with Fe/Al = 0.20 and Fe/Al = 0.65 only contain mononuclear and binuclear Fe species, respectively, as active reaction species, and then their TOF for N_2O decomposition at 500 °C under dry and wet conditions can be calculated by the equation, $C/(W/F_{N_2O}) \times 1/n_{\text{active site}}$, where the former term $(C/(W/F_{N_2O}))$ is the rate of N_2O decomposition over Fe/ZSM5 catalysts, and C, W, F_{N_2O} and $n_{\text{active site}}$ are the fractional conversion, the catalyst weight (g), the flow rate of N_2O (mol/s), and the concentration of active site (mol/g), respectively [38,55]. The results for Fe-ZSM-5-SSIE samples with Fe/Al = 0.20 and Fe/Al = 0.65 were ca. $1.5 \times 10^{-3}\ s^{-1}$ and $1.8 \times 10^{-3}\ s^{-1}$, respectively under dry condition, and $0.3 \times 10^{-3}\ s^{-1}$ and $0.6 \times 10^{-3}\ s^{-1}$, respectively under wet condition. They clearly indicate that binuclear Fe species for the catalyst containing higher Fe/Al, 0.65 are more active for N_2O decomposition than mononuclear Fe ones, particularly under the wet condition.

4. Conclusion

The catalytic decomposition of nitrous oxide in the presence of excess oxygen with and without water vapor was carried out over Fe-ZSM-5-WIE and -SSIE catalysts. It has been observed that the Fe-ZSM-5-SSIE catalysts generally achieve a high performance of N_2O decomposition compared to that of Fe-ZSM-5-WIE, and the catalysts also reveal a distinctive decomposition activity with respect to Fe/Al ratio of the catalysts. As the content of Fe over the Fe-ZSM-5-SSIE catalysts increases up to the ratio of Fe/Al = 0.49, the activity steeply increases, and when Fe/Al > 0.49, the activity gradually increases and then levels off to about 80% of N_2O conversion to N_2. However, the decomposition activity of N_2O over Fe-ZSM5-WIE catalysts decreases when Fe/Al > 0.46, mainly due to the formation of Fe_2O_3 particles on the catalyst surface confirmed by XRD, UV–vis and XAFS.

Based upon the results from the theoretical and experimental confirmation of EXAFS function $\chi(k)$ for α-Fe_2O_3 and the imaginary parts of Fe–Fe, Fe–Al, and Fe–Si backscatterings calculated by an *ab initio* EXAFS code FEFF8, the second neighboring atom at ca. 2.7 Å in the RSF spectra for the Fe-ZSM-5-SSIE catalysts may be attributed to the Fe–Fe backscattering, not Fe–Al and Fe–Si. EXAFS analyses also reveal that a unique Fe ion over Fe-ZSM-5-SSIE catalysts prepared in the present study may mainly be Fe binuclear species such as oxygen-bridged binuclear Fe complex, not larger multinuclear Fe clusters, even with the high Fe loadings on the catalyst surface. However, Fe-ZSM-5-SSIE and -WIE catalysts with low Fe loadings were found to contain mononuclear Fe species as the major Fe species confirmed by the amount of H_2 consumption through TPR analysis. On the basis of these results, turnover frequencies (TOF) of the N_2O decomposition over Fe-ZSM-5-SSIE samples with Fe/Al = 0.20 and Fe/Al = 0.65 were ca. $1.5 \times 10^{-3}\ s^{-1}$ and $1.8 \times 10^{-3}\ s^{-1}$, respectively, under dry condition, and $0.3 \times 10^{-3}\ s^{-1}$ and $0.6 \times 10^{-3}\ s^{-1}$, respectively, under wet condition. It can be concluded that binuclear Fe species is an active reaction site for N_2O decomposition and is responsible for the high catalytic performance of Fe-ZSM-5-SSIE (Fe/Al > 0.2) even with water in the feed gas stream.

Acknowledgement

The authors are grateful to the authorities of Pohang Light Source (PLS) for X-ray absorption spectroscopic measurements and financial support of this work was partially provided by the National Research Laboratory Program (ROA-2007-000-20050-0) of the Korea Science and Engineering Foundation.

References

[1] G.I. Panov, A.K. Uriarte, M.A. Rodkin, V.I. Sobolev, Catal. Today 41 (1998) 365.
[2] K.A. Dubkov, V.I. Sobolev, E.P. Talsi, M.A. Rodkin, N.H. Watkins, A.A. Shteinman, G.I. Panov, J. Mol. Catal. A 123 (1997) 155.
[3] D. Meloni, R. Monaci, V. Solinas, G. Berlier, S. Bordiga, I. Rossetti, C. Oliva, L. Forni, J. Catal. 214 (2003) 169.
[4] V. Sobolev, G. Panov, A. Kharitonov, V. Romannikov, A. Volodin, K. Ione, J. Catal. 139 (1993) 435.
[5] X. Feng, W.K. Hall, Catal. Lett. 41 (1996) 45.
[6] H.Y. Chen, W.M.H. Sachtler, Catal. Lett. 50 (1998) 125.
[7] G.I. Panov, V.I. Sobolev, A.S. Kharitonov, J. Mol. Catal. 61 (1990) 85.
[8] E.M. El-Malki, R.A. van Santen, W.M.H. Sachtler, Microporous Mesoporous Mater. 35 (2000) 235.
[9] C. Sang, C.R.F. Lund, Catal. Lett. 70 (2000) 165.
[10] J.C. Groen, A. Brückner, E. Berrier, L. Maldonado, J.A. Moulijn, J. Pérez-Ramírez, J. Catal. 243 (2006) 212.
[11] D.A. Bulushev, L. Kiwi-Minsker, A. Renken, J. Catal. 222 (2004) 389.
[12] J. Pérez-Ramírez, J. Catal. 227 (2004) 512.
[13] G.D. Pirngruber, L. Frunz, J.A.Z. Pieterse, J. Catal. 243 (2006) 340.
[14] X. Feng, W.K. Hall, J. Catal. 166 (1997) 368.
[15] P. Marturano, A. Kogelbauer, R. Prins, J. Catal. 190 (2000) 460.
[16] H.-Y. Chen, W.M.H. Sachtler, Catal. Today 42 (1998) 73.

[17] T.V. Voskoboinikov, H.-Y. Chen, W.M.H. Sachtler, Appl. Catal. B 19 (1998) 279.
[18] H.-Y. Chen, El-M. El-Malki, X. Wang, R.A. van Santen, W.M.H. Sachtler, J. Mol. Catal. A 162 (2000) 159.
[19] P. Marturano, L. Drozdova, A. Kogelbauer, R. Prins, J. Catal. 192 (2000) 236.
[20] A.A. Battiston, J.H. Bitter, F.M.F. de Groot, A.R. Overweg, O. Stephan, J.A. van Bokhoven, P.J. Kooyman, C. van der Spek, G. Vankó, D.C. Koningsberger, J. Catal. 213 (2003) 251.
[21] A.A. Battiston, J.H. Bitter, W.M. Heijboer, F.M.F. de Groot, D.C. Koningsberger, J. Catal. 215 (2003) 279.
[22] L.J. Lobree, I.-C. Hwang, J.A. Reimer, A.T. Bell, J. Catal. 186 (1999) 242.
[23] S.H. Choi, B.R. Wood, J.A. Ryder, A.T. Bell, J. Phys. Chem. B 107 (2003) 11843.
[24] G.D. Pirngruber, P.K. Roy, R. Prins, Phys. Chem. Chem. Phys. 8 (2006) 3939.
[25] W. Heijboer, "New Frontiers in X-ray Spectroscopy of FeZSM-5", University of Utrecht, PhD thesis (2005).
[26] K. Yoshizawa, T. Yumura, Y. Shiota, T. Yamabe, Bull. Chem. Soc. Jpn. 73 (2000) 29.
[27] A. Heyden, B. Peters, A.T. Bell, F.J. Keil, J. Phys. Chem. 109 (2005) 1857.
[28] T. Nobukawa, M. Yoshida, K. Okumura, K. Tomishige, K. Kunimori, J. Catal. 229 (2005) 347.
[29] N. Hansen, A. Heyden, A.T. Bell, F.J. Keil, J. Phys. Chem. C 111 (2007) 2092.
[30] R. Joyner, M. Stockenhuber, J. Phys. Chem. B. 103 (1999) 5963.
[31] R. Joyner, M. Stockenhuber, Catal. Lett. 45 (1997) 15.
[32] J.-H. Park, C.H. Park, I.-S. Nam, Appl. Catal. A 277 (2004) 271.
[33] J.-H. Park, H.J. Park, J.H. Baik, I.-S. Nam, C.-H. Shin, J.-H. Lee, B.K. Cho, S.H. Oh, J. Catal. 240 (2006) 47.
[34] M. Newville, P. Livins, Y. Yacoby, J.J. Rehr, E.A. Stern, Phys. Rev. B 47 (1993) 14126.
[35] P.A. O'Day, J.J. Rehr, S.I. Zabinsky, G.E. Brown Jr., J. Am. Chem. Soc. 116 (1994) 2938.
[36] J. Leglise, J.O. Petunchi, W.K. Hall, J. Catal. 86 (1984) 392.
[37] C.M. Fu, V.N. Korchak, W.K. Hall, J. Catal. 68 (1981) 166.
[38] El-M. El-Malki, R.A. van Santen, W.M.H. Sachtler, J. Catal. 196 (2000) 212.
[39] F. Kapteijn, G. Marbán, J. Rodriguez-Mirasol, J.A. Moulijn, J. Catal. 167 (1997) 256.
[40] W.K. Hall, X. Feng, J. Dumesic, R. Watwe, Catal. Lett. 52 (1998) 13.
[41] G.D. Pirngruber, J.-D. Grunwaldt, P.K. Roy, J.A. van Bokhoven, O. Safonova, P. Glatzel, Catal. Today 126 (2007) 127.
[42] R.W. van den Brink, S. Booneveld, J.R. Pels, D.F. Bakker, M.J.F.M. Verhaak, Appl. Catal. B 32 (2001) 73.
[43] S. Bordiga, R. Buzzoni, F. Geobaldo, C. Lamberti, E. Giamello, A. Zecchina, G. Leofanti, G. Petrini, G. Tozzola, G. Vlaic, J. Catal. 158 (1996) 486.
[44] H.H. Tippins, Phys. Rev. B 1 (1970) 126.
[45] P. Ratnasamy, R. Kumar, Catal. Today 9 (1991) 341.
[46] P. Marturano, L. Drozdová, G.D. Pirngruber, A. Kogelbauer, R. Prins, Phys. Chem. Chem. Phys. 3 (2001) 5585.
[47] L.X. Chen, T. Liu, M.C. Thurnauer, R. Csencsits, T. Rajh, J. Phys. Chem. B 106 (2002) 8539.
[48] A.L. Ankudinov, J.J. Rehr, S.R. Bare, Chem. Phys. Lett. 316 (2000) 495.
[49] G. Draeger, W. Czolbe, J.A. Leiro, Phys. Rev. B 45 (1992) 8283.
[50] T.E. Westre, P. Kennepohl, J.G. DeWitt, B. Hedman, K.O. Hodgson, E.I. Solomon, J. Am. Chem. Soc. 119 (1997) 6297.
[51] E. Hensen, Q. Zhu, P.-H. Liu, K.-J. Chao, R. van Santen, J. Catal. 226 (2004) 466.
[52] E. Hensen, Q. Zhu, M. Hendrix, A. Overweg, P. Kooyman, M. Sychev, R. van Santen, J. Catal. 221 (2004) 560.
[53] M. Schwidder, M.S. Kumar, K. Klementiev, M.M. Pohl, A. Brückner, W. Grünert, J. Catal. 231 (2005) 314.
[54] T. Nobukawa, K. Sugawara, K. Okumura, K. Tomishige, K. Kunimori, Appl. Catal. B 70 (2007) 342.
[55] G.D. Pirngruber, M. Luechinger, P.K. Roy, A. Cecchetto, P. Smirniotis, J. Catal. 224 (2004) 429.